Violation of the ultrastructural size principle in the dorsolateral prefrontal cortex underlies working memory impairment in the aged common marmoset (Callithrix jacchus)

Courtney Glavis-Bloom[1]*†, Casey R. Vanderlip[1]†,
Sammy Weiser Novak[2], Masaaki Kuwajima[3], Lyndsey Kirk[3],
Kristen M. Harris[3], Uri Manor[2] and John H. Reynolds[1]

[1]Salk Institute for Biological Studies, Systems Neurobiology Laboratory, La Jolla, CA, United States, [2]Salk
Institute for Biological Studies, Waitt Advanced Biophotonics Center, La Jolla, CA, United States,
[3]Department of Neuroscience, Center for Learning and Memory, University of Texas at Austin, Austin,
TX, United States

Morphology and function of the dorsolateral prefrontal cortex (dlPFC), and corresponding working memory performance, are affected early in the aging process, but nearly half of aged individuals are spared of working memory deficits. Translationally relevant model systems are critical for determining the neurobiological drivers of this variability. The common marmoset (Callithrix jacchus) is advantageous as a model for these investigations because, as a non-human primate, marmosets have a clearly defined dlPFC that enables measurement of prefrontal-dependent cognitive functions, and their short (∼10 year) lifespan facilitates longitudinal studies of aging. Previously, we characterized working memory capacity in a cohort of marmosets that collectively covered the lifespan, and found age-related working memory impairment. We also found a remarkable degree of heterogeneity in performance, similar to that found in humans. Here, we tested the hypothesis that changes to synaptic ultrastructure that affect synaptic efficacy stratify marmosets that age with cognitive impairment from those that age without cognitive impairment. We utilized electron microscopy to visualize synapses in the marmoset dlPFC and measured the sizes of boutons, presynaptic mitochondria, and synapses. We found that coordinated scaling of the sizes of synapses and mitochondria with their associated boutons is essential for intact working memory performance in aged marmosets. Further, lack of synaptic scaling, due to a remarkable failure of synaptic mitochondria to scale with presynaptic boutons, selectively underlies age-related working memory impairment. We posit that this decoupling results in mismatched energy supply and demand, leading to impaired synaptic transmission. We also found that aged marmosets have fewer synapses in dlPFC than young, though the severity of synapse loss did not predict whether aging occurred with or without cognitive impairment. This work identifies a

novel mechanism of synapse dysfunction that stratifies marmosets that age with cognitive impairment from those that age without cognitive impairment. The process by which synaptic scaling is regulated is yet unknown and warrants future investigation.

1. Introduction

Working memory, the ability to maintain and manipulate information for short durations, critically depends on the dorsolateral prefrontal cortex (dlPFC) (Funahashi et al., 1989; Arnsten et al., 2012). Within the dlPFC, neurons in layer III fire repeatedly in the absence of selective sensory stimuli to hold information in working memory (Goldman-Rakic, 1995; Arnsten et al., 2012). The properties of this elevated firing is an area of active research and multiple models have been proposed (Constantinidis et al., 2018; Miller et al., 2018; Wang, 2021). Importantly, these models posit that stimulus-selective changes in ongoing neural activity are necessary to support working memory. This activity is, by necessity, reliant on synaptic efficacy, the ability of synapses to efficiently transfer information between neurons. This efficacy is essential to the formation and maintenance of neural networks that underlie learning and memory (Kennedy, 2016). Therefore, intact memory is dependent on synaptic efficacy (Borczyk et al., 2021), and reduced synaptic efficacy results in decreased information transfer and memory impairment (Świetlik et al., 2019). Thus it is unsurprising that elevated firing that supports working memory is vulnerable to changes that compromise synaptic efficacy, such as those that occur with aging. Indeed, the dlPFC undergoes morphological and functional changes with age that correlate with working memory impairment (Morrison and Baxter, 2012; Upright and Baxter, 2021). For example, in macaque monkeys, aging and working memory impairment are associated with synapse loss (Hao et al., 2007; Peters et al., 2008). Selective loss of small synapses accounts for this loss (Dumitriu et al., 2010), and it is these synapses that are thought to be essential for the elevated firing in dlPFC that supports working memory (Kasai et al., 2003; Wang et al., 2011; Arnsten et al., 2012).

Elevated firing is metabolically demanding due, in part, to the high energy demands of synaptic transmission (Attwell and Laughlin, 2001), and this energy is primarily generated by presynaptic mitochondria (Rossi and Pekkurnaz, 2019; Pekkurnaz and Wang, 2022). Presynaptic mitochondria are a critical source of energy needed to support synaptic efficacy, and the demand for their energy is especially acute during elevated firing such as that which supports working memory. Therefore, it is unsurprising that the dlPFC has increased mitochondrial density compared to other cortical regions (Chandrasekaran et al., 1992; Arnsten et al., 2012).

As mitochondria age, they become impaired in their ability to provide energy, resulting in a reduced energy budget for the brain (Yao et al., 2010; Todorova and Blokland, 2017; Olesen et al., 2020). Aging is also associated with structural changes to mitochondria that are indicative of dysfunction. For example, in aged macaques with working memory impairment, there is increased prevalence of toroidal-shaped mitochondria in presynaptic boutons from layer III dlPFC. These boutons that contain toroidal-shaped mitochondria are associated with markers of decreased synaptic strength (Hara et al., 2014).

The ultrastructural size principle describes the fact that strong correlations between synaptic components (e.g., presynaptic mitochondria and synapses) and the size of the associated presynaptic bouton are critical for synaptic efficacy (Pierce and Mendell, 1993; Pierce and Lewin, 1994; Meyer et al., 2014). These correlations are upheld during periods of synaptic growth and remodeling (Meyer et al., 2014). Specifically, the elevated firing that supports working memory is defined by extended periods of synaptic activity during which the energy demands of synapses change rapidly. Under these conditions, it is especially important that each component of the synaptic complex varies in lockstep to meet the fluctuating energy demands of synapses and maintain effective synaptic transmission (Smith et al., 2016). The present study tests the hypothesis that violations of the ultrastructural size principle undermine synaptic efficacy, thereby contributing to synaptic dysfunction, and consequently, age-related working memory impairment. These violations would be observed as weak or absent correlations between the sizes of synaptic components in aged animals with working memory impairment compared to aged animals without cognitive impairment and young animals.

To test this hypothesis, we utilized three dimensional reconstruction from serial section electron microscopy (3DEM) to quantify structural correlates of synaptic strength in layer III dlPFC from three marmosets that varied in age and working memory capacity. Using this approach, we quantified synaptic components including presynaptic boutons, presynaptic mitochondria, and synapses, and investigated their relationship with each other. We identified a pronounced violation of the ultrastructural size principle that is specific to the aged marmoset with working memory impairment.

2. Materials and methods

2.1. Subjects

Two aged common marmosets (Callithrix jacchus, 9.3 year-old male, 9.6 year-old female), previously assessed on a working memory task (Glavis-Bloom et al., 2022), and one young control

(1.3 year-old female), were used for this study. All experiments were conducted in compliance with the Institutional Animal Care and Use Committee of the Salk Institute for Biological Studies and conformed to NIH guidelines.

2.2. Cognitive testing

Working memory ability of the aged marmosets was assessed using the Delayed Recognition Span Task (DRST; Figure 1A), as described in detail previously (Glavis-Bloom et al., 2022). Briefly, the DRST was initiated by the marmoset touching a blue square stimulus in the center of the screen. Then, a single black and white stimulus, selected randomly without replacement from a bank of 400, was displayed on the screen in one of nine possible locations, also selected randomly. When the marmoset touched this first stimulus, a small liquid reward was dispensed. Following a 2-s delay, during which the screen was blank, a forced choice presented two alternatives: the original stimulus appearing in its original location, and a second, novel stimulus, appearing in a different location. If the marmoset selected the novel object (non-match-to-sample), a correct response was logged, a liquid reward was dispensed, and another 2-s delay ensued. Following the delay, the first two stimuli appeared in their original locations, and a third, novel stimulus, also appeared, in a pseudo randomly chosen location. The marmoset was again rewarded for choosing the novel stimulus. Novel stimuli were added after subsequent delays until the trial was terminated in one of three ways: (1) the marmoset made nine correct selections in a row; (2) the marmoset failed to make a selection within 12 s (i.e., omitted); and (3) the marmoset made an incorrect response (i.e., selected a non-novel stimulus). Marmosets were neither water nor food restricted.

2.3. Tissue collection

Even brief hypoxic episodes affect the structural integrity of synaptic ultrastructure which then precludes accurate ultrastructural measurements (Tao-Cheng et al., 2007). Therefore, we adapted a rodent hypoxia-resistant transcardiac perfusion euthanasia protocol (Kuwajima et al., 2013) for use in marmosets.

Alfaxalone (12 mg/kg, i.m.) and diazepam (2 mg/kg, i.m.) were administered to induce anesthesia, and atropine (0.02 mg/kg, i.m.) was administered to reduce saliva. Marmosets were deeply anesthetized with isoflurane (3–5%) delivered with oxygen (1– 1.5 L/min) *via* a mask over their nose and mouth, and then intubated and ventilated (2.75 cc tidal volume, 60 breaths/min) to ensure oxygenation throughout the procedure. Once a deep surgical plane of anesthesia was reached, the thoracic cavity was opened with a lateral incision under the rib cage and a midline incision over the sternum. The pleura was bluntly dissected to expose the heart and lungs, and retractors were placed to maintain access to the thoracic cavity. The right atrium was clipped with iris scissors, and a blunt 18 gauge needle with warmed (37°C), oxygenated Krebs-Ringer Carbicarb (KRC) buffer flowing was inserted into the left ventricle. After 3 s, the marmosets were perfused with 2% formaldehyde and 2.5% glutaraldehyde in 0.1 M cacodylate buffer (pH: 7.35). After 1 h of perfusion, the brain was
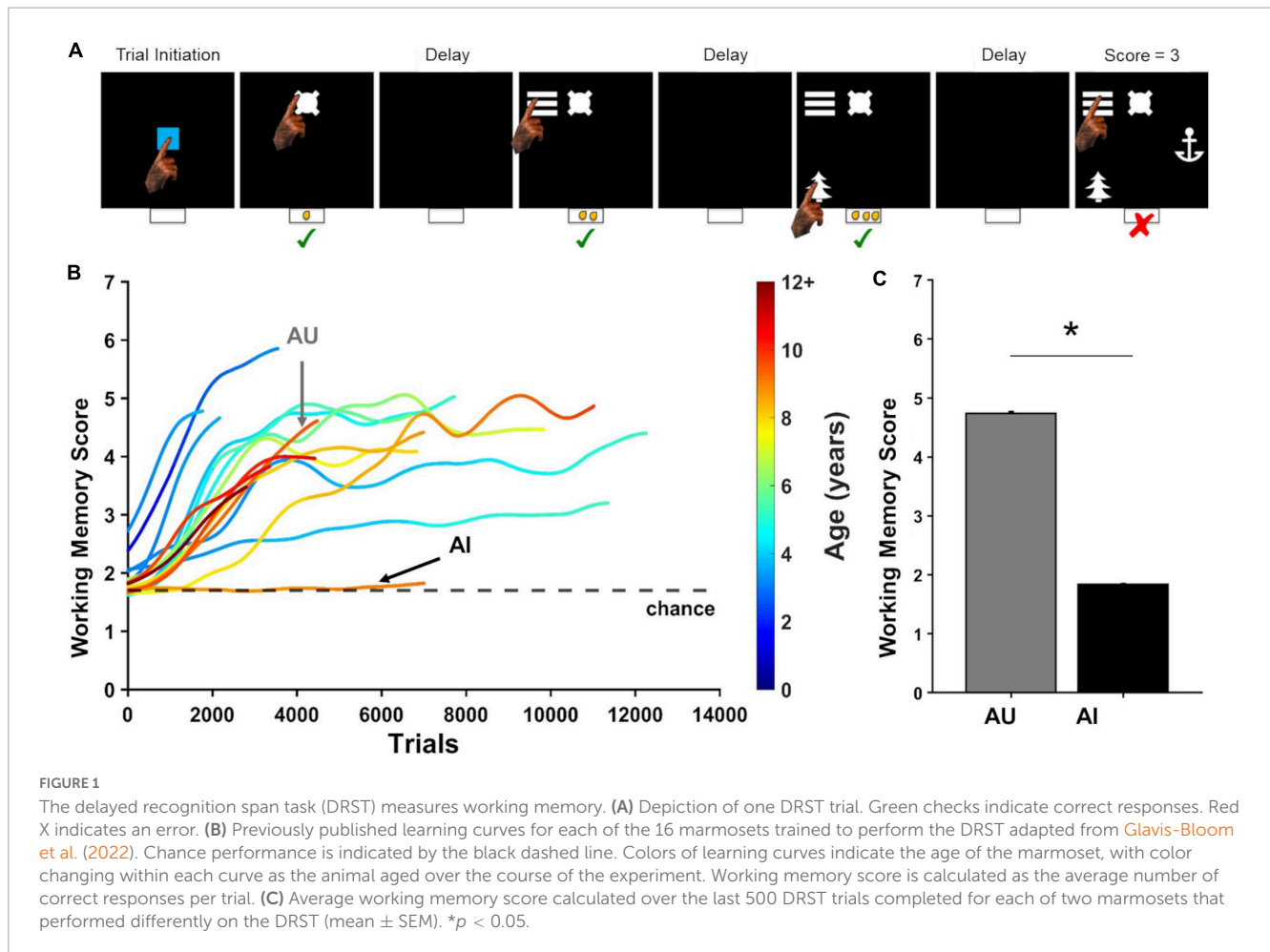
harvested, post-fixed in the same fixation solution at 4°C for 48 h, and then processed for electron microscopy.

2.4. Electron microscopy

Materials were sourced from Electron Microscopy Sciences unless noted otherwise. Brains were processed into coronal sections of 100 μm thickness using a vibrating microtome (Leica VT1000S, Leica Microsystems, Wetzlar, Germany). Sections that included the dorsolateral prefrontal cortex (dlPFC) area 46 (Paxinos et al., 2012) were selected for further processing. These sections were microdissected perpendicular to the cortical surface to produce dlPFC samples that contained both the cortical surface and deeper cortical layers. These approximately 0.5 mm tall and 3 mm wide microdissected dlPFC samples were transferred into glass vials and rinsed with ice cold 0.1 M sodium cacodylate with 3 mM calcium chloride for 15 min three times before staining and post-fixation with reduced osmium (1.5% osmium tetroxide, 1% potassium ferrocyanide, 3 mM calcium chloride, 0.1 M sodium cacodylate) for 45 min in the dark at room temperature. Samples were rinsed three times with ice cold deionized water and left overnight in 1% aqueous uranyl acetate in the dark at 4°C. Samples were rinsed three times briefly in deionized water before serial dehydration in ascending concentrations of ice cold ethanol (20, 50, 70, 80, 90, 100, 100; 10 min per change). Samples were then infiltrated with Eponate 12 resin (Pelco; Product No. 18012) hard formulation, in a 1:1 mix with anhydrous ethanol overnight on a rotating mixer. The following day, the samples were further infiltrated with 2:1:resin:ethanol mix for 2 h, then transferred from their vials into shallow polypropylene bottle caps filled with pure resin for 2 h. Fresh resin was exchanged and the samples were further infiltrated for 2 h before embedding in a silicone rubber mold and polymerization for 48 h at 70°C.

Semi-thin (0.7–1 μm) sections extending from the cortical surface to the deeper cortical layers were collected using a diamond knife (DiATOME, Hatfield, PA, USA) on an ultramicrotome (Leica UC7). Layer III was identified by neuroanatomical landmarks on the semi-thin sections, including distance from the cortical surface and density of neuronal somas (Yuasa et al., 2010; Paxinos et al., 2012). Then, the blockface was carefully trimmed using a 90° diamond trim tool to a dimension of approximately 0.6 mm × 0.2 mm in layer III, and a ribbon of approximately 200 serial sections (55–70 nm) was collected onto a silicon chip partially immersed in the knife boat and, as the water level was lowered using the peristaltic pump, the sections dried down onto the silicon substrate. The chip was mounted on an aluminum stub using a sticky carbon tab, and loaded into a scanning electron microscope (SEM; Sigma VP scanning electron microscope, Zeiss). Images were collected using a Gatan backscattered electron detector at a working distance of 7 mm and an accelerating voltage of 3 kV. Image maps of the series at variable resolutions were assembled using the extended raster scanning and control system (Eberle et al., 2015) (Atlas5, FIBICS, Ottawa, ON, Canada) and layer III was identified.

A region from layer III was selected for imaging by overlaying a numbered grid with 50 μm × 50 μm spacing, and randomly selecting a number from the grid. These potential

FIGURE 1
The delayed recognition span task (DRST) measures working memory. **(A)** Depiction of one DRST trial. Green checks indicate correct responses. Red X indicates an error. **(B)** Previously published learning curves for each of the 16 marmosets trained to perform the DRST adapted from Glavis-Bloom et al. (2022). Chance performance is indicated by the black dashed line. Colors of learning curves indicate the age of the marmoset, with color changing within each curve as the animal aged over the course of the experiment. Working memory score is calculated as the average number of correct responses per trial. **(C)** Average working memory score calculated over the last 500 DRST trials completed for each of two marmosets that performed differently on the DRST (mean ± SEM). *$p < 0.05$.

imaging regions were evaluated every 10 sections through the ribbon at an intermediate resolution to ensure that the series would be devoid of somas and blood vessels to ensure equivalent analysis of neuropil across samples. The chosen imaging regions were imaged through 41 consecutive serial sections with a pixel size of 2 nm. The image sequence was contrast normalized using the scikit-image implementation of CLAHE (van der Walt et al., 2014) and rigidly aligned using TrakEM2 in Fiji (Cardona et al., 2012). These volumes were cropped to a minimum contiguous cube of roughly aligned data with no padding. Fine image stack alignment was accomplished using SWiFT-IR[1] as deployed on 3DEM.org using the TACC compute resource Stampede 2 (Litvina et al., 2019), with final contiguous volumes formed of approximately 20 μm × 20 μm × 2.5 μm.

2.5. Image segmentation and reconstruction

The image stacks were imported into Volume Annotation and Segmentation Tool (VAST Lite) (Berger et al., 2018) for three-dimensional reconstruction of presynaptic boutons and

their mitochondria, and the associated synapse surface area. We employed similar sampling methods to prior work in macaque monkeys (Hara et al., 2011, 2014, 2016; Fehr et al., 2022). The experimenter performing the segmentations was blind to the subject-identifying information of the images. The middle image of each stack ("reference image") was selected, and a central region of dimensions 18 μm × 9 μm was identified. To quantify within-subject variability utilizing a repeated measures approach, this 162 μm^2 analysis region was divided into four non-overlapping regions of interest (ROIs), each 40.5 μm^2 (9 μm × 4.5 μm). Each of these four ROIs had two inclusion borders and two exclusion borders (**Figure 2A**) to standardize the volume of neuropil analyzed for each sample. Presynaptic boutons were identified on the reference region and were included if they were either fully inside a ROI, or partially crossed an inclusion border. These included boutons were segmented on the reference section and throughout their entirety through the image stack. As in prior work, presynaptic boutons were defined as containing three or more presynaptic vesicles on the reference section (Hara et al., 2014, 2016). Presynaptic mitochondria and synapses associated with these boutons were also segmented (**Figure 2B**). All boutons, whether they were non-synaptic or formed the presynaptic side of asymmetric or symmetric synapses, were included. There were no axosomatic or axoaxonic synapses.
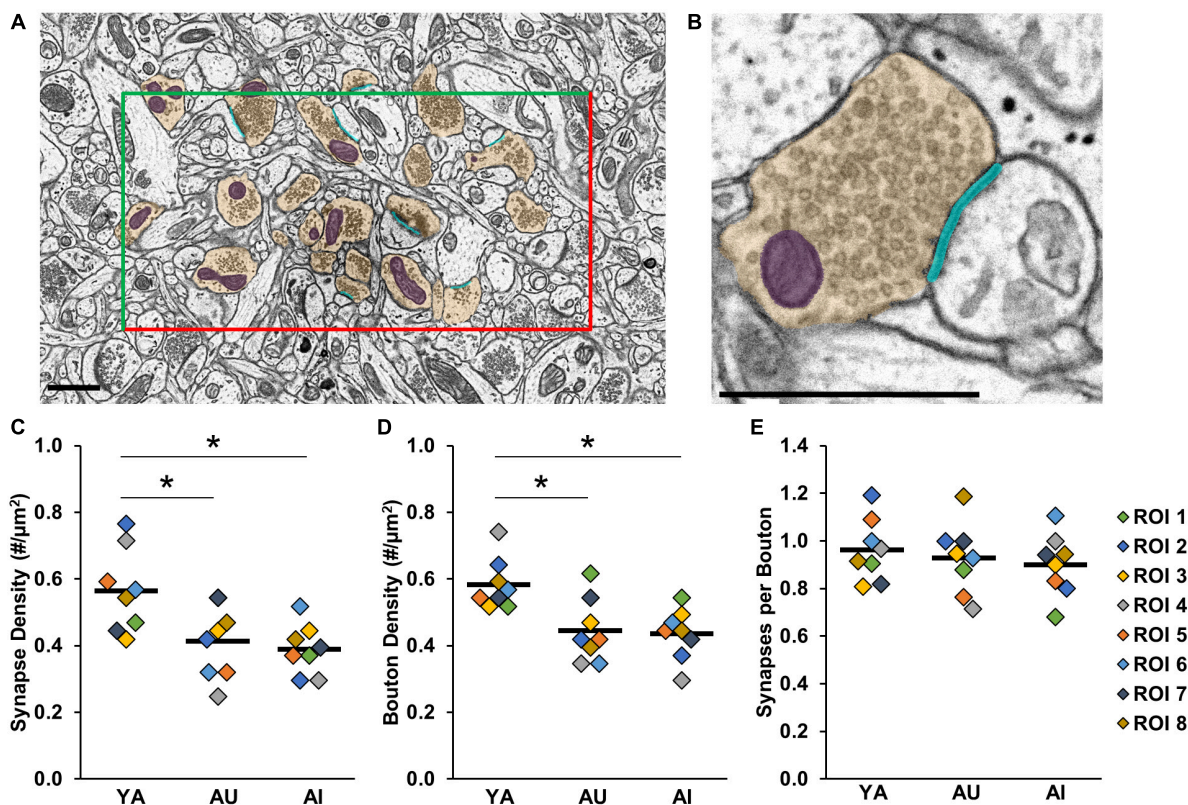
---

1 https://ieeexplore.ieee.org/document/8010595

FIGURE 2

Synapse and bouton density are decreased in aged marmosets compared to young, regardless of working memory capacity. **(A)** Reference section with one region of interest (ROI) outlined by two inclusion (green) and two exclusion (red) lines. Included presynaptic boutons are segmented in yellow, synapses in cyan, mitochondria in purple. Scale bar = 1 μm. **(B)** Zoomed in view of one synaptic complex. Colors and scale bar as in panel **(A)**. **(C)** Synapse density **(D)** Bouton density **(E)** Synapses per bouton. There were an equivalent number of synapses per bouton across animals. In panels **(C–E)**, colored diamonds represent measures taken in each of the ROIs. Horizontal black bars represent average across the ROIs. *$p < 0.05$.

Three dimensional modeling software (Blender)[2] was used with the Geometry-preserving Adaptive Mesher plugin (GAMer) (Lee et al., 2019; Lees et al., 2020) to generate smoothed, biologically accurate contours (i.e., "meshes"). Bouton and mitochondria surface area and volume measurements were taken from the meshes, and the mitochondria were classified by their morphology (straight, curved, toroidal). In alignment with prior work, mitochondria that were bent less than 90 degrees were classified as straight, mitochondria that bent 90 degrees or more were classified as curved, and toroidal-shaped (sometimes referred to as donut-shaped in the literature),were classified as toroidal (Hara et al., 2014, 2016). Synapse surface area was quantified by measuring synapse lengths (i.e., apposition of the presynaptic active zone and postsynaptic density) from each image on which they appeared, and multiplying by the section thickness. Approximately 160 boutons were analyzed from each subject.

2.6. Statistical analyses

Data were analyzed using MATLAB (Mathworks, Natick, MA, USA). Shapiro-Wilk tests for normality revealed that the data

were normally distributed, and so parametric statistical analyses were performed. Associations between two variables were assessed using Pearson correlations and Model II regressions. Strengths of the correlations were compared with Fisher Z-tests. Two-way analysis of variance (ANOVA) tests were used to assess two factor interactions. One-way ANOVAs with Tukey's HSD *post-hoc* tests were used to identify within-factor differences. Within-subject variability was quantified with a repeated measures approach, with eight regions of interest per animal. $P < 0.05$ was considered significant.

3. Results

3.1. Aging heterogeneously affects working memory capacity

Behavioral findings from a large group of marmosets, including the two aged monkeys used in this study, are described in detail elsewhere (Glavis-Bloom et al., 2022). Learning curves from each of these 16 animals are recapitulated in **Figure 1B** which illustrates the heterogeneity of working memory performance in the cohort of marmosets we tested that collectively cover the lifespan. Here, we focus on two aged marmosets that performed differently on the

DRST; one successfully learned the rules of the DRST and reached a high level of performance (Aged Unimpaired; AU), while the other, similarly aged monkey, failed to learn the DRST, and continued to perform at chance levels of accuracy even after extensive experience on the task (Aged Impaired; AI). On the last 500 DRST trials each marmoset performed, the AI marmoset's average Working Memory Score (number of items identified correctly on a given trial) was significantly lower than that of the AU marmoset [**Figure 1C**; Welch's t-test: $t(538) = 23.03$, $p = 3.45 \times 10^{-82}$].

3.2. Age-related working memory impairment is associated with reduced coordination of pre- and post-synaptic components

Synaptic efficacy is critically dependent on the correlated sizes of synaptic components including boutons, synapses, and mitochondria. This coordinated scaling is known as the ultrastructural size principle. Whether and how the ultrastructural size principle is upheld with age and in cognitive impairment, however, is unknown. To investigate the synaptic changes underlying this cognitive impairment, we used 3DEM to quantify synapses, boutons, and presynaptic mitochondria in layer III of the dlPFC from three marmosets: a young adult (YA), an aged cognitively unimpaired animal (AU), and an aged cognitively impaired animal (AI).

Prior observations in macaques and humans show that there is reduced synaptic density in layer III of the dlPFC with age, and this reduction is more severe in humans and non-human primates with age-related cognitive impairment (Peters et al., 2008; Dumitriu et al., 2010; Boros et al., 2017). Marmosets are shorter-lived than are macaques and humans, raising the question of whether this same pattern of synapse loss is observed in aged animals and if it is more pronounced in aged marmosets exhibiting cognitive impairment. Consistent with prior work, we found a significant age-related decrease in synapse density [**Figure 2C**; one-way ANOVA: $F_{(2)} = 6.62$, $p = 0.006$]. However, synapse density was reduced in both AU and AI, and did not vary significantly with cognitive impairment (Tukey's HSD: YA vs. AU: $p = 0.02$; YA vs. AI: $p = 0.008$; AU vs. AI: $p = 0.89$). We then quantified bouton density and the number of synapses per bouton for each marmoset to evaluate whether the age-related reduction in synapse density was due to a loss of boutons, a reduction in the number of synapses per bouton, or a combination of the two. Similar to synapse density, we found an overall decrease in bouton density in both aged animals (**Figure 2D**; one-way ANOVA: $F_{(2)} = 8.05$, $p = 0.003$) and no variation with working memory impairment (Tukey's HSD: YA vs. AU: $p = 0.008$; YA vs. AI: $p = 0.005$; AU vs. AI: $p = 0.97$). Furthermore, there was an equivalent number of synapses per bouton across animals (**Figure 2E**; one-way ANOVA: $F_{(2)} = 0.41$, $p = 0.67$). Together, these results demonstrate synapse and bouton loss in aged marmosets compared to young that does not change with cognitive status.

This leaves open the possibility that, rather than being driven by synapse or bouton number, working memory impairments might stem instead from a dysfunction of the synapse itself. In particular, we hypothesized that a failure of coordination in the

size of the components of the synaptic complex—violations of the ultrastructural size principle, might underlie cognitive impairment. To test this, we quantified synapse and bouton size in each of our marmosets (**Figure 3**), and then investigated whether violations of the ultrastructural size principle predicted cognitive performance.

Consistent with prior microscopy studies from layer III dlPFC in macaques and humans, we observe an increased average synapse size in aged animals compared to young that is exacerbated with age-related cognitive impairment (**Figure 4A**; one-way ANOVA: $F_{(2)} = 31.23$, $p < 0.0001$; Tukey's HSD *post hoc*: YA vs. AU: $p = 0.001$; YA vs. AI: $p < 0.0001$; AU vs. AI: $p = 0.004$). Prior work has shown that the overall increase in average synapse size is due to a selective loss of small, plastic synapses with age, and further loss of these particular synapses with cognitive impairment (Dumitriu et al., 2010; Boros et al., 2017). Bouton size was also greater in aged compared to young marmosets but did not significantly depend on cognitive status (**Figure 4B**; one-way ANOVA: $F_{(2)} = 19.62$, $p < 0.0001$; Tukey's HSD: YA vs. AU: $p = 0.0003$, YA vs. AI: $p = < 0.0001$; AU vs. AI: $p = 0.54$). Since the ultrastructural size principle states that synapse and bouton sizes are highly correlated, it is unexpected that synapse size varied significantly between AU and AI, and bouton size did not.

To assess whether the reduced coordination between synapse and bouton size is specific for the AI marmoset, or whether it is ubiquitous with aging but exacerbated with age-related working memory impairment, we compared the ratios and correlations of synapse and bouton surface area across animals. The ratio of summed synapse surface area to bouton surface area was consistent between YA and AU, whereas it was larger in the AI marmoset (**Figure 4C**; one-way ANOVA: $F_{(2)} = 4.87$, $p = 0.02$; Tukey's HSD: YA vs. AU: $p = 1.00$; YA vs. AI: $p = 0.03$; AU vs. AI: $p = 0.03$). We found strong correlations in all subjects (**Figure 4D**; YA: $r_p = 0.68$, $p < 0.0001$; AU: $r_p = 0.80$, $p < 0.0001$; AI: $r_p = 0.61$, $p < 0.0001$), and that the correlation was significantly weaker in AI compared to AU (Fisher Z transformation: YA vs. AU: $p = 0.024$; YA vs. AI: $p = 0.32$; AU vs. AI: $p = 0.003$). In violation of the ultrastructural size principle, weaker correlation between boutons and synapses, along with disproportional scaling between these two components may reflect synaptic dysfunction that underlies the working memory impairment in AI.

3.3. Synaptic boutons that contain mitochondria are selectively vulnerable to synaptic dysfunction in an aged marmoset with working memory impairment

We next asked whether the presence of presynaptic mitochondria affected the synapse to bouton ratio. First, we found no changes in the frequency of mitochondria containing boutons in any of the conditions (One-way ANOVA: $F_{(2)} = 0.75$, $p = 0.49$). This opens the possibility that synapse and bouton surface area may vary as a function of the presence or absence of presynaptic mitochondria, and also with age and working memory impairment.

In regards to bouton size, we found that, across all animals, boutons with presynaptic mitochondria are larger than boutons
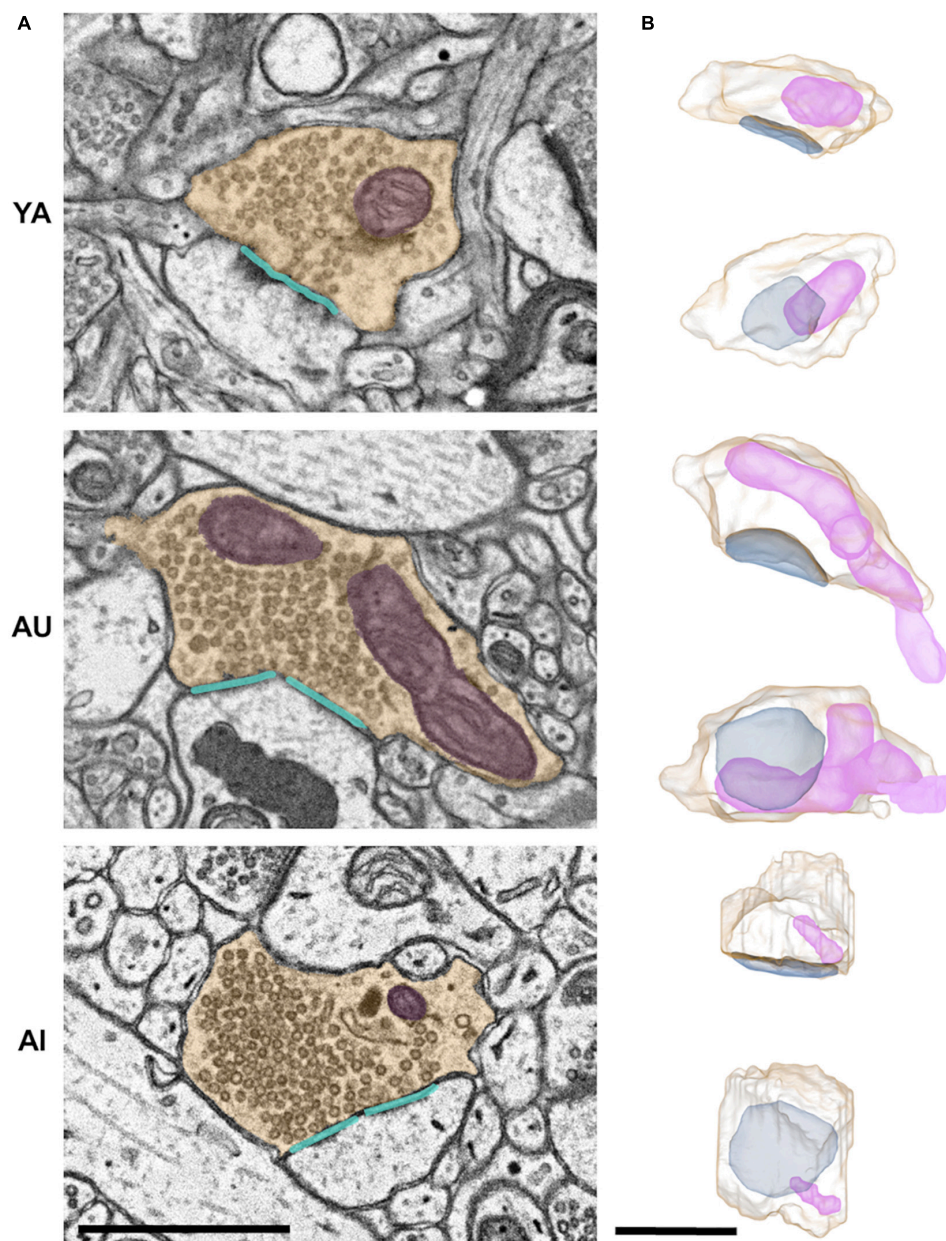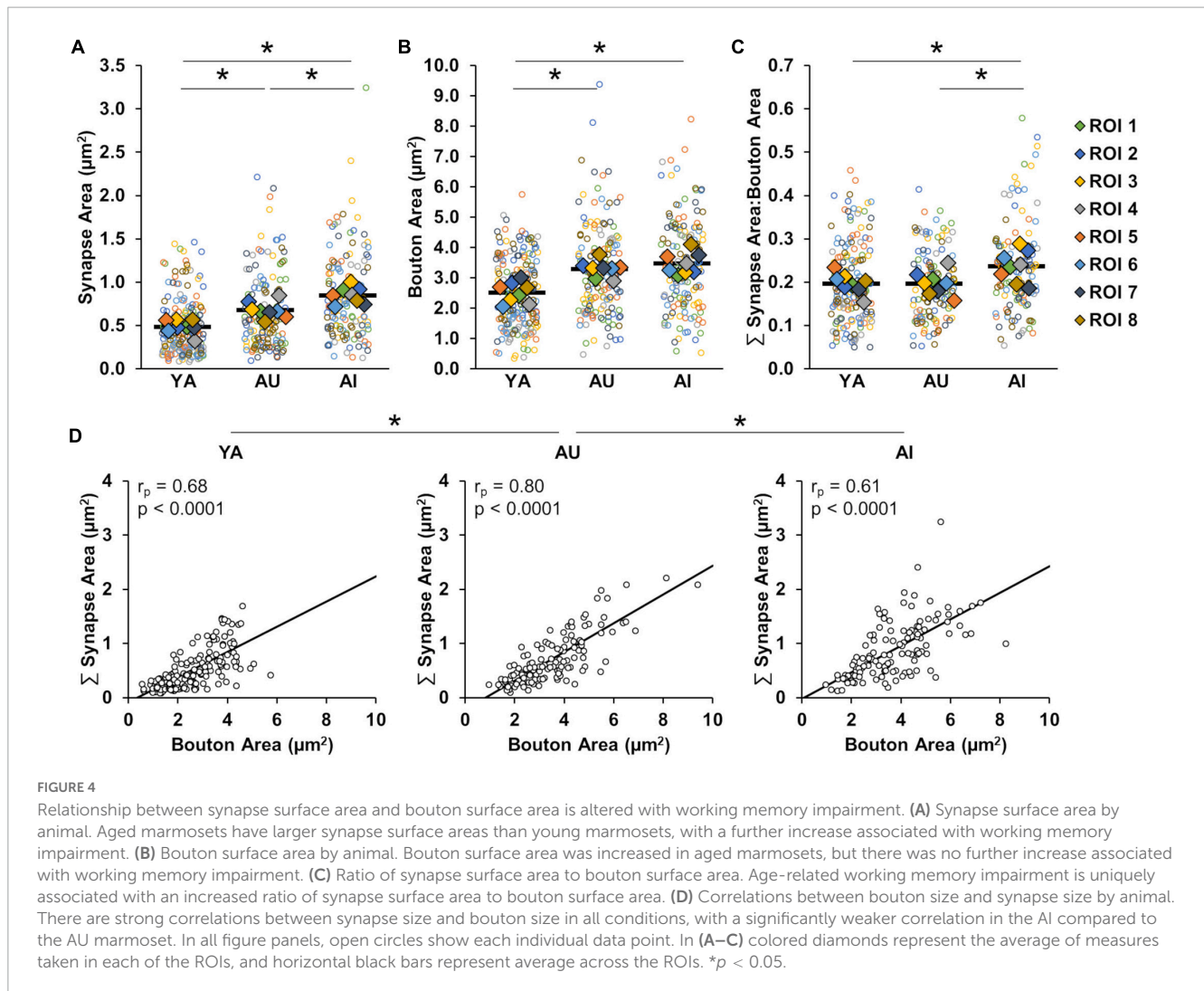
FIGURE 3
Synaptic complex segmentations and reconstructions. **(A)** Two-dimensional segmentations, and **(B)** paired orthogonal projections of representative synaptic complexes from the young adult (YA; top row), aged unimpaired (AU; middle row), and aged impaired (AI; bottom row) marmosets. Presynaptic boutons are shown in yellow, mitochondria in purple, synapses in cyan. Scale bars are 1 μm.

without presynaptic mitochondria (**Figure 5A**; Two-way ANOVA: mitochondria presence $F_{(1)} = 160.31$, $p = 1.42 \times 10^{-15}$; Tukey's HSD: $p = 1.63 \times 10^{-10}$). Analyzed separately, however, there were differences between the animals both for boutons with mitochondria and boutons without mitochondria [Two-way ANOVA: animal $F_{(2)} = 16.29$, $p = 6.69 \times 10^{-6}$; interaction (mitochondria presence × animal) $F_{(2)} = 8.49$, $p = 0.0008$]. For boutons without mitochondria, those in the AI marmoset were significantly larger than in YA and AU (Tukey's HSD; YA vs. AU: $p = 0.35$, YA vs. AI: $p = 0.0008$, AU vs. AI: $p = 0.02$). For boutons with mitochondria, boutons were significantly larger in both aged marmosets compared to young, however, AI marmoset boutons

with mitochondria were significantly smaller than those in AU (Tukey's HSD; YA vs. AU: $p = 3.68 \times 10^{-5}$, YA vs. AI: $p = 0.02$, AU vs. AI: $p = 0.03$).

We applied these same analyses to assess the effects of mitochondrial presence on synapse size, and found a similar pattern of results [**Figure 5B**; Two-way ANOVA: mitochondria presence $F_{(1)} = 78.70$, $p < 0.0001$; animal $F_{(2)} = 33.58$, $p < 0.0001$; interaction $F_{(2)} = 4.21$, $p = 0.02$]. Specifically, across all animals, synapses associated with presynaptic mitochondria were larger than those that were not (Tukey's HSD: $p < 0.0001$). Also, synapses without associated presynaptic mitochondria were larger with cognitive impairment (Tukey's HSD; YA vs. AU: $p = 0.72$,

FIGURE 4

Relationship between synapse surface area and bouton surface area is altered with working memory impairment. **(A)** Synapse surface area by animal. Aged marmosets have larger synapse surface areas than young marmosets, with a further increase associated with working memory impairment. **(B)** Bouton surface area by animal. Bouton surface area was increased in aged marmosets, but there was no further increase associated with working memory impairment. **(C)** Ratio of synapse surface area to bouton surface area. Age-related working memory impairment is uniquely associated with an increased ratio of synapse surface area to bouton surface area. **(D)** Correlations between bouton size and synapse size by animal. There are strong correlations between synapse size and bouton size in all conditions, with a significantly weaker correlation in the AI compared to the AU marmoset. In all figure panels, open circles show each individual data point. In **(A–C)** colored diamonds represent the average of measures taken in each of the ROIs, and horizontal black bars represent average across the ROIs. *$p < 0.05$.

YA vs. AI: $p < 0.0001$, AU vs. AI: $p = 0.0001$), whereas synapses associated with mitochondria were larger in both aged animals relative to YA, and did not vary with cognitive status (Tukey's HSD; YA vs. AU: $p = 0.01$, YA vs. AI: $p = 0.0001$, AU vs. AI: $p = 0.72$). Taken together, these results show that the presence or absence of presynaptic mitochondria has differential effects on structural correlates of synaptic strength, and these effects vary as a function of age and cognitive impairment.

To resolve the question of whether the presence or absence of presynaptic mitochondria renders associated boutons and synapses vulnerable to dysfunction, we calculated the ratio of synapse to bouton size separately for boutons without mitochondria and boutons with mitochondria (**Figure 5C**). We found a significant increase in the synapse to bouton size ratio of the AI marmoset compared to the YA and AU animals in the boutons containing mitochondria, but not in the boutons without mitochondria [One-way ANOVA: without mitochondria: $F_{(2)} = 2.18$, $p = 0.14$, with mitochondria: $F_{(2)} = 6.77$, $p = 0.005$; Tukey's HSD: YA vs. AU: $p = 0.83$; YA vs. AI: $p = 0.03$; AU vs. AI: $p = 0.03$]. Therefore, mitochondria likely contribute to synaptic dysfunction in AI, but how this occurs is an open question.

3.4. Decorrelation between presynaptic boutons and mitochondria is associated with synaptic dysfunction in age-related working memory impairment

Synaptic transmission is metabolically demanding and this energy is primarily supplied by mitochondria (Attwell and Laughlin, 2001) that are essential for synaptic efficacy and stability (Smith et al., 2016; Lees et al., 2020). While the percentage of boutons that contained mitochondria did not vary across animals (one-way ANOVA: $F_{(2)} = 0.75$, $p = 0.49$), there are several mechanisms by which mitochondria could underlie synaptic dysfunction, including: (1) low mitochondrial density, (2) dysmorphic mitochondria, (3) reduced mitochondrial size, and (4) improper scaling of mitochondria and bouton size. We investigate each of these in-turn, below.

We first quantified the number of mitochondria per bouton for each animal, and found that the average did not vary across animals (**Figure 6A**: one-way ANOVA: $F_{(2)} = 1.72$, $p = 0.20$).

Since mitochondrial size correlates with energy production (Ivannikov et al., 2013; Ashaber et al., 2020), we next quantified mitochondria surface area to determine if smaller
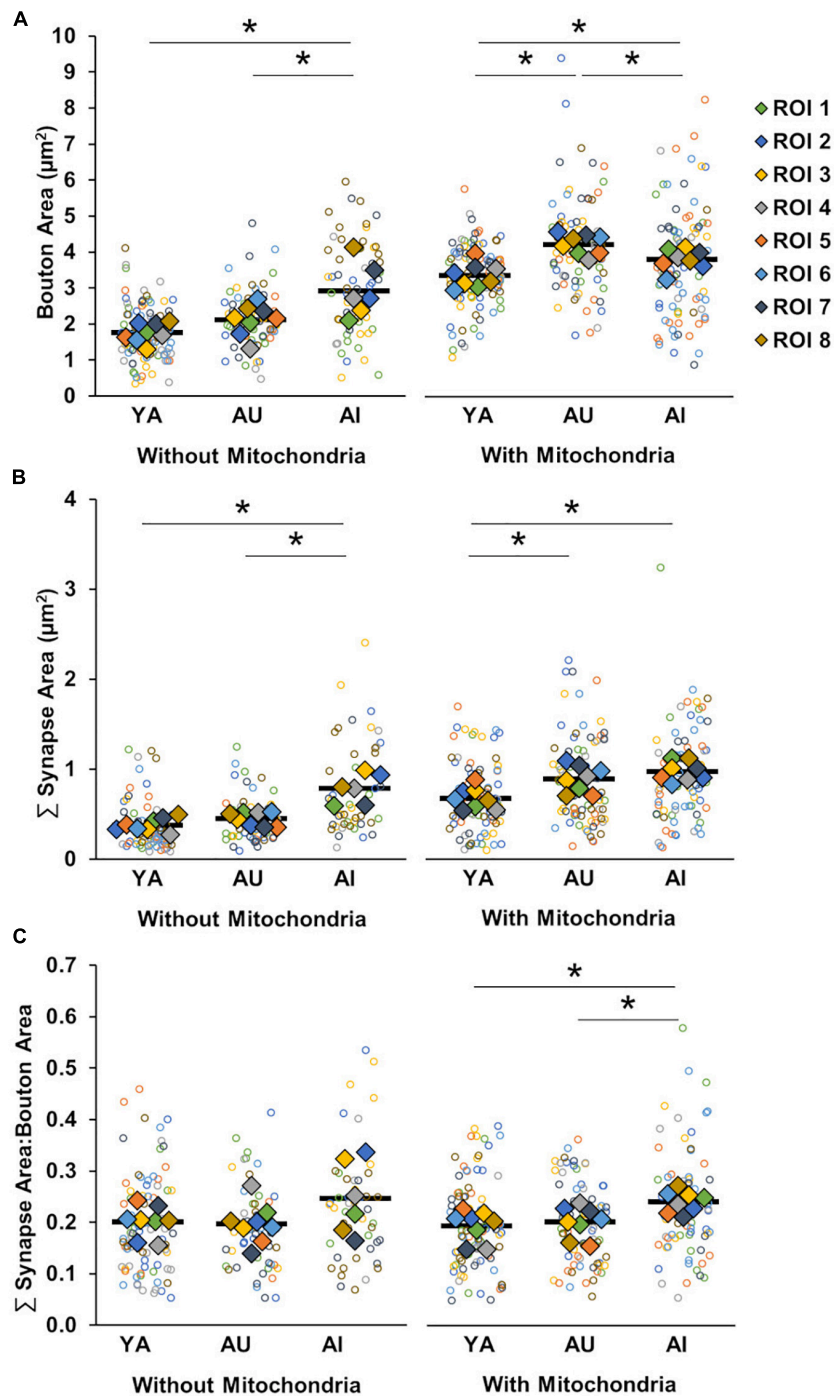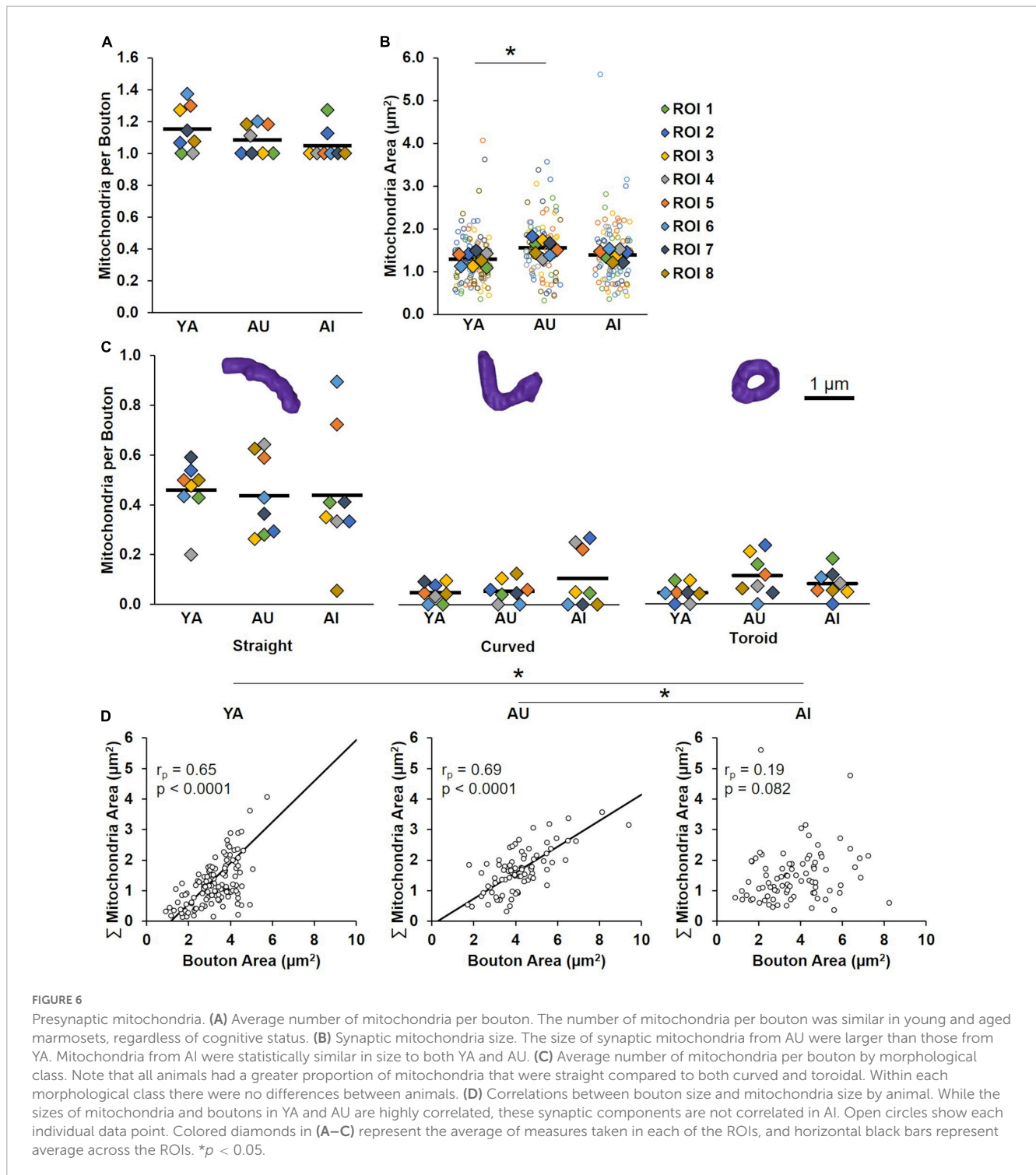
FIGURE 5

Boutons and synapses with and without mitochondria. **(A)** Bouton size by absence or presence of presynaptic mitochondria. Boutons without presynaptic mitochondria were larger in AI compared to YA and AU. Boutons with presynaptic mitochondria were larger in both aged marmosets than the young, with further enlargement in AU compared to AI. **(B)** Summed synapse surface area by absence or presence of presynaptic mitochondria. Synapses without associated presynaptic mitochondria were larger in AI compared to YA and AU, while synapses with associated presynaptic mitochondria were larger in aged marmosets, regardless of cognitive status. **(C)** Ratio of synapse surface area to bouton area by absence or presence of presynaptic mitochondria. The ratio of synapse size to bouton size is significantly larger in the AI marmoset compared to YA and AU only when presynaptic mitochondria were present. Open circles show each individual data point, colored diamonds represent the average of measures taken in each of the ROIs, and horizontal black bars represent average across the ROIs. *$p < 0.05$.

mitochondria are responsible for synaptic dysfunction in the AI marmoset. However, we found no differences between AI marmoset mitochondria and YA and AU mitochondria (**Figure 6B**; one-way ANOVA: $F_{(2)} = 5.84$, $p = 0.01$;

Tukey's HSD: YA vs. AU: $p = 0.01$, YA vs. AI: $p = 0.44$, AU vs. AI: $p = 0.11$).

Prior work demonstrates that dysmorphic mitochondria (e.g., toroids) are indicative of impaired energy production

FIGURE 6
Presynaptic mitochondria. **(A)** Average number of mitochondria per bouton. The number of mitochondria per bouton was similar in young and aged marmosets, regardless of cognitive status. **(B)** Synaptic mitochondria size. The size of synaptic mitochondria from AU were larger than those from YA. Mitochondria from AI were statistically similar in size to both YA and AU. **(C)** Average number of mitochondria per bouton by morphological class. Note that all animals had a greater proportion of mitochondria that were straight compared to both curved and toroidal. Within each morphological class there were no differences between animals. **(D)** Correlations between bouton size and mitochondria size by animal. While the sizes of mitochondria and boutons in YA and AU are highly correlated, these synaptic components are not correlated in AI. Open circles show each individual data point. Colored diamonds in **(A–C)** represent the average of measures taken in each of the ROIs, and horizontal black bars represent average across the ROIs. *$p < 0.05$.

(Liu and Hajnóczky, 2011; Ahmad et al., 2013; Galloway and Yoon, 2013; Glancy et al., 2020). To test whether mitochondria morphology contributes to synaptic dysfunction in the AI marmoset, we quantified the number of mitochondria per bouton that were straight, curved, or toroidal in each animal. We found that while there were overall more straight mitochondria than curved or toroidal (Tukey's HSD: straight vs. curved: $p = 9.56 \times 10^{-10}$; straight vs. toroidal: $p = 9.56 \times 10^{-10}$; curved vs. toroidal: $p = 0.95$), there were no differences between animals [**Figure 6C**; two-way

ANOVA: morphology $F_{(1)} = 72.94$, $p = 4.01 \times 10^{-17}$; animal $F_{(2)} = 0.24$, $p = 0.79$; interaction $F_{(2)} = 0.47$, $p = 0.75$].

Finally, we tested the hypothesis that mitochondria do not scale properly with bouton size. We found similarly strong correlations between these structures in YA and AU (**Figure 6D**; YA: $r_p = 0.65$, $p < 0.0001$, AU: $r_p = 0.69$, $p < 0.0001$; Fisher Z transformation: YA vs. AU: $p = 0.66$). Remarkably, there was no correlation between bouton size and mitochondria size in AI ($r_p = 0.19$, $p = 0.082$; Fisher Z transformation: YA vs. AI: $p = 0.0002$, AU
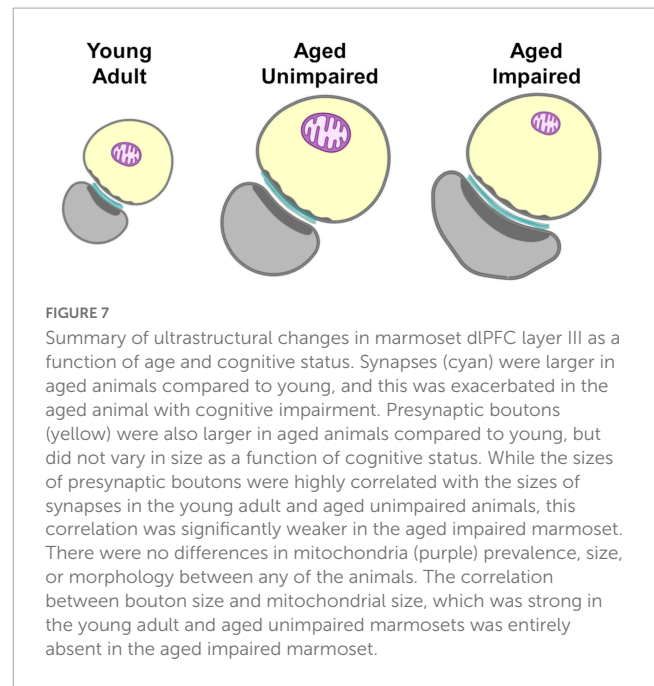
vs. AI: $p < 0.0001$). These results support our hypothesis that decorrelation between mitochondria and their boutons underlies synaptic dysfunction in AI.

4. Discussion

Like humans (Nyberg et al., 2020), marmosets exhibit heterogeneity in their cognitive aging profiles (Glavis-Bloom et al., 2022). Therefore, the marmoset is a powerful model for understanding the neural mechanisms that drive this variability and can help identify what causes some individuals to sustain age-related cognitive impairment, while others remain unaffected. In this study we examined the ultrastructural features of synaptic complexes and how they change as a function of age and age-related cognitive impairment. We used electron microscopy to visualize and quantify synaptic components in layer III of the dlPFC from one young adult and two aged marmosets. Each of the aged marmosets had previously undergone working memory assessment. One exhibited working memory function comparable to young adult marmosets, while an age-matched animal exhibited profound working memory impairment (Glavis-Bloom et al., 2022). The main feature that distinguished the aged marmoset with cognitive impairment from that without was a novel form of synaptic dysfunction: violation of the ultrastructural size principle (Figure 7). In particular, we found that while the sizes of presynaptic boutons were highly correlated with the sizes of synapse surface areas in a young adult and aged unimpaired animal, this correlation was significantly weaker in the age-matched impaired animal. Further, among boutons that contained mitochondria, the correlation between bouton size and mitochondrial size, which was strong in the young adult and aged unimpaired animal was entirely absent in the aged impaired animal. Since the size of mitochondria is proportional to their energy production (Ivannikov et al., 2013; Ashaber et al., 2020), and the size of boutons is proportional to their energy demand (for review see Harris et al., 2012), we posit that in the aged impaired animal, energy supply does not equal demand on a bouton by bouton basis, resulting in a breakdown of synaptic transmission. These findings are important in that they reveal a novel form of synaptic dysfunction that may contribute to age-related cognitive impairment. This study is, to our knowledge, the first to find evidence that age-related working memory impairments may stem from a violation of the ultrastructural size principle, and is the first characterization of synaptic ultrastructure in cognitively profiled marmosets.

4.1. Aged marmosets have synapse loss consistent in severity to aged macaques

We focused here on the dlPFC because it is critical for working memory, and morphological and functional changes in this region have been observed early in the aging process (Morrison and Baxter, 2012; Upright and Baxter, 2021). Consistent with observations in macaques (Bertoni-Freddari et al., 2007; Peters et al., 2008; Dumitriu et al., 2010; Morrison and Baxter, 2012; Crimins et al., 2017), we find that aged marmosets have a

FIGURE 7
Summary of ultrastructural changes in marmoset dlPFC layer III as a function of age and cognitive status. Synapses (cyan) were larger in aged animals compared to young, and this was exacerbated in the aged animal with cognitive impairment. Presynaptic boutons (yellow) were also larger in aged animals compared to young, but did not vary in size as a function of cognitive status. While the sizes of presynaptic boutons were highly correlated with the sizes of synapses in the young adult and aged unimpaired animals, this correlation was significantly weaker in the aged impaired marmoset. There were no differences in mitochondria (purple) prevalence, size, or morphology between any of the animals. The correlation between bouton size and mitochondrial size, which was strong in the young adult and aged unimpaired marmosets was entirely absent in the aged impaired marmoset.

marked (28%) reduction in synapse density compared to young. Whereas prior studies in macaques, using large sample sizes, report significant negative correlations between synapse density in dlPFC and age-related cognitive impairment (Peters et al., 2008; Dumitriu et al., 2010), we did not find that synapse density varied as a function of cognitive status in the aged marmosets. It is possible that our limited sample size and individual variability might contribute to this difference with the literature (see Section "4.5. Limitations," below). Despite the lack of synapse density differences between the two aged animals, we find that the remaining synapses are larger in aged monkeys than young, and this is significantly exacerbated in the aged animal with working memory impairment. This aligns with prior work in macaques that shows that increased average synapse size is due to a selective loss of small synapses associated with thin spines that are critical for supporting working memory (Bertoni-Freddari et al., 2007; Dumitriu et al., 2010; Arnsten et al., 2012). To our knowledge, this is the first report of age-related synapse loss in the marmoset.

4.2. Weaker correlation between the sizes of synapses and boutons with age-related cognitive impairment

Investigations of age-related changes to structural correlates of synaptic efficacy historically have focused on either presynaptic or postsynaptic analyses. The fact that pre and postsynaptic components are linearly related in size in young animals, thus aligning with the ultrastructural size principle (Lisman and Harris, 1993; Pierce and Mendell, 1993; Pierce and Lewin, 1994), leaves open the question of how these scaling relationships change as a function of age and cognitive impairment. Consistent with prior work in aged macaques (Cork et al., 1990; Crimins et al., 2017), we found that aged marmoset presynaptic boutons were larger than young. Furthermore, congruent with the ultrastructural size

principle and prior work in aged macaque dlPFC, there were strong linear relationships between synapse and bouton sizes in each of the marmosets. However, this correlation was significantly weaker in the aged marmoset with cognitive impairment compared to the aged unimpaired marmoset. Additionally, the ratio of synapse to bouton size was conserved between the young adult and aged unimpaired marmoset, but was significantly larger in the aged animal with working memory impairment, as compared to each of the other animals. This violation of the ultrastructural size principle indicates a form of synaptic dysfunction.

4.3. Boutons containing mitochondria selectively account for violation of the ultrastructural size principle in age-related working memory impairment

The elevated firing rates that underlie working memory involve substantial synaptic activity. This activity is metabolically demanding, and the required energy is primarily supplied by synaptic mitochondria (Li et al., 2020). We thus hypothesized that a mismatch between energy supply and demand would be especially detrimental to maintenance of elevated firing, and is therefore a mechanism by which synaptic dysfunction occurs. To test this hypothesis, we divided synaptic complexes into two subgroups depending on whether the presynaptic bouton contained mitochondria or did not. We found that the increased ratio of synapse to bouton size in the AI marmoset was explained selectively by synaptic complexes with boutons that contained mitochondria. These findings lend support to the idea that mitochondria contribute to synaptic dysfunction underlying age-related working memory impairment, and leaves open the question of how this occurs.

4.4. Evidence that mitochondria contribute to age-related working memory impairment through mismatched energy supply for synaptic demand

We proposed four explanations for how mitochondria could underlie synaptic dysfunction through mismatched energy supply for synaptic demand: (1) low mitochondrial density, (2) dysmorphic mitochondria, (3) reduced mitochondrial size, and (4) improper scaling. We tested each proposed mechanism by measuring structural correlates of mitochondrial energy production.

First, we hypothesized that the AI marmoset had fewer mitochondria per bouton compared to the YA and AU animals, which could lead to insufficient energy for synapses to function properly. However, we found that mitochondrial density was equivalent across all animals, which means that lower density of synaptic mitochondria cannot explain synaptic dysfunction in the AI marmoset. Our findings are consistent with prior work reporting that young and aged macaques have similar mitochondrial density

in dlPFC (Bertoni-Freddari et al., 2007; Hara et al., 2014), but differ from this prior research in that presynaptic mitochondrial density in macaque dlPFC was positively correlated with working memory capacity (Hara et al., 2014). This correlation, however, was specific to mitochondria classified as healthy (i.e., straight), whereas density of mitochondria with other morphologies (e.g., curved, toroidal) were not predictive of memory capacity. Therefore, the health of the existing mitochondria could explain mismatched energy supply for synaptic demand in age-related working memory impairment.

Mitochondrial morphology is indicative of their overall health and ability to generate energy. Specifically, toroidal-shaped mitochondria produce less energy than straight mitochondria (Liu and Hajnóczky, 2011; Ahmad et al., 2013; Galloway and Yoon, 2013; Morrison and Baxter, 2014; Glancy et al., 2020), and so we hypothesized that an increased number of toroidal-shaped mitochondria in the AI marmoset might lead to insufficient energy supply for synaptic demand and contribute to synaptic dysfunction. Consistent with prior research in macaques (Hara et al., 2014), we found more straight mitochondria than curved and toroidal-shaped mitochondria in each marmoset, and no difference in the prevalence of toroidal-shaped mitochondria between young and aged animals. Additionally, both Hara et al. and our work find no correlation between the prevalence of toroidal-shaped mitochondria and performance on challenging working memory tasks using delayed non-matching rules. However, Hara et al. (2014) did find a negative correlation between toroidal-shaped mitochondria prevalence and performance on a delayed response task, but this was due to large between-animal variability that led to no difference in delayed response performance between young and aged macaques. Together, these results suggest that toroidal mitochondria presence may account for working memory performance in cases where individual variability is most pronounced, such as tasks of moderate difficulty. Mitochondrial size directly correlates with markers of synaptic efficacy (Pierce and Lewin, 1994; Ivannikov et al., 2013; Smith et al., 2016). Therefore, reduced mitochondrial size may lead to reduced energy production, resulting in mismatched synaptic energy supply and demand. However, our results do not support reduced mitochondrial size as a mechanistic explanation for synaptic dysfunction because the average size of mitochondria in the aged animal with working memory impairment was equivalent to mitochondrial size in both of the other animals. However, the aged animal with conserved working memory had significantly larger mitochondria than the young animal, which reflects alignment with the ultrastructural size principle; the size of presynaptic mitochondria should increase to maintain correlation with the age-related increase in bouton size. The fact that bouton size increased in the aged impaired marmoset but mitochondria size did not suggests that synaptic dysfunction may result from improper scaling of mitochondria in the aged impaired animal.

Coordinated scaling of mitochondria with presynaptic boutons is critical for maintaining effective synaptic transmission, especially during elevated firing that demands large amounts of energy. We found that in the young adult and the aged animal without cognitive impairment, there were similarly strong correlations between mitochondrial and presynaptic bouton size. Remarkably though, in the aged animal with working memory impairment, there was no correlation between mitochondria

and presynaptic bouton size, demonstrating violation of the ultrastructural size principle.

We postulate that this violation causes dysfunctional neuronal signaling. Mitochondrial size is proportional to energy production (Ivannikov et al., 2013; Ashaber et al., 2020), and increased size is directly associated with increased neurotransmitter release and synaptic efficacy (Ivannikov et al., 2013; Cserép et al., 2018). Additionally, mitochondrial size rapidly adapts to differing firing rates, growing in response to elevated firing (Thomas et al., 2019), such as that which supports working memory in the dlPFC (Goldman-Rakic, 1995; Curtis and D'Esposito, 2003; Wang et al., 2011; Arnsten et al., 2012; Wimmer et al., 2014). Therefore, in healthy conditions such as YA and AU, mitochondria may dynamically regulate the strength of synaptic connections. However, if mitochondrial size is not correlated with other synaptic components, as is the case with AI, neurotransmitter release will not reflect presynaptic input. Specifically, when mitochondria are disproportionately small for the associated bouton, insufficient release of neurotransmitters may result in reduced signal transduction between neurons. Conversely, disproportionately large mitochondria could lead to overly exuberant release of neurotransmitters and hyperexcitability. Together, dysregulation between adjacent neurons has the potential to disrupt entire circuits and impair working memory. Therefore, understanding the processes that govern the coordination between synaptic components to maintain synaptic efficacy is critical to elucidating the mechanisms of cognitive aging.

4.5. Limitations

The primary limitation of this study is its limited sample size. We selected the aged animals used in this study from our cohort of marmosets that conjointly cover the lifespan and have been tested on the DRST (Glavis-Bloom et al., 2022). The cognitive aging heterogeneity within our cohort resembles that observed in macaques and humans (Moss et al., 2007; Nyberg et al., 2020). As a result, we were able to take advantage of this opportunity and identify two age-matched animals with significantly different cognitive abilities, enabling this unique investigation. In some respects, our findings differ from macaque studies that utilized large sample sizes. This is particularly the case with synapse density, where we did not recapitulate an association between synapse loss and age-related cognitive impairment (Peters et al., 2008; Dumitriu et al., 2010). While it is important to note that our small sample size and individual variability might contribute to this difference with the published literature, there are several things that somewhat mitigate this concern. First, we did have statistical power to recapitulate age-related synapse loss, and the degree of synapse loss (28%) is remarkably matched with what has been shown previously in macaques (Peters et al., 2008; Dumitriu et al., 2010). Second, there was a profound difference in cognitive ability between the two aged marmosets. If this difference was attributed to a difference in synapse loss, we anticipate the magnitude of the cognitive difference would be comparable to the magnitude of the synapse loss difference. Instead, we found no difference in the degree of synapse loss between the two aged animals. Finally, we did find a remarkable difference between the aged animals in the form of complete decorrelation of the sizes of mitochondria

and boutons. While the volume of tissue we analyzed from each animal is large for high-resolution electron microscopy work, it is relatively small compared to what can be analyzed using lower resolution techniques. We maximized use of the tissue volume by analyzing both asymmetric and symmetric synapses, which are both important for working memory. Further evaluation is needed to determine if the ultrastructural size principle applies similarly to both excitatory and inhibitory synapses. Finally, while synaptic structure and function are highly related (Meyer et al., 2014), the fact that electron microscopy is conducted on post-mortem tissue means that the conclusions we draw between structure and function are correlative rather than direct. Complimentary studies in the future could provide a more macroscopic view and direct investigation of function.

5. Conclusion

Here we have identified a novel mechanism by which age-related working memory impairment may emerge: violation of the Ultrastructural Size Principle. We posit that this violation leads to synaptic dysfunction through mismatched energy supply and demand, disrupting the elevated firing necessary for working memory. To our knowledge, this work also represents the first examination of synaptic ultrastructure in the aged common marmoset. Finally, linking ultrastructure to cognitive capacity further validates the marmoset as a model for understanding the neural underpinnings of aging, and could reveal why aging itself is the biggest risk factor for neurodegenerative diseases.

Data availability statement

The raw data supporting the conclusions of this article will be made available by the authors, without undue reservation.

Ethics statement

The animal study was reviewed and approved by the Institutional Animal Care and Use Committee of the Salk Institute for Biological Studies.

Author contributions

CG-B and JR contributed to conception of the study. CG-B, CV, and SW performed the study and wrote the first draft of the manuscript. CG-B and CV performed data analyses. All authors contributed to the design of the study, manuscript revision, read, and approved the submitted version.

Funding

Conflict of interest

The authors declare that the research was conducted in the absence of any commercial or financial relationships that could be construed as a potential conflict of interest.

Publisher's note

All claims expressed in this article are solely those of the authors and do not necessarily represent those of their affiliated organizations, or those of the publisher, the editors and the reviewers. Any product that may be evaluated in this article, or claim that may be made by its manufacturer, is not guaranteed or endorsed by the publisher.

References

Ahmad, T., Aggarwal, K., Pattnaik, B., Mukherjee, S., Sethi, T., Tiwari, B. K., et al. (2013). Computational classification of mitochondrial shapes reflects stress and redox state. *Cell Death Dis.* 4, e461–e461. doi: 10.1038/cddis.2012.213

Arnsten, A. F. T., Wang, M. J., and Paspalas, C. D. (2012). Neuromodulation of thought: Flexibilities and vulnerabilities in prefrontal cortical network synapses. *Neuron* 76, 223–239. doi: 10.1016/j.neuron.2012.08.038

Ashaber, M., Zalányi, L., Pálfi, E., Stuber, I., Kovács, T., Roe, A. W., et al. (2020). Synaptic organization of cortico-cortical communication in primates. *Eur. J. Neurosci.* 52, 4037–4056. doi: 10.1111/ejn.14905

Attwell, D., and Laughlin, S. B. (2001). An energy budget for signaling in the grey matter of the brain. *J. Cereb. Blood Flow Metab.* 21, 1133–1145. doi: 10.1097/00004647-200110000-00001

Berger, D. R., Seung, H. S., and Lichtman, J. W. (2018). VAST (volume annotation and segmentation tool): Efficient manual and semi-automatic labeling of large 3D image stacks. *Front. Neural Circuits* 12:88. doi: 10.3389/fncir.2018.00088

Bertoni-Freddari, C., Fattoretti, P., Giorgetti, B., Grossi, Y., Balietti, M., Casoli, T., et al. (2007). Preservation of mitochondrial volume homeostasis at the early stages of age-related synaptic deterioration. *Ann. N. Y. Acad. Sci.* 1096, 138–146. doi: 10.1196/annals.1397.079

Borczyk, M., Radwanska, K., and Giese, K. P. (2021). The importance of ultrastructural analysis of memory. *Brain Res. Bull.* 173, 28–36. doi: 10.1016/j.brainresbull.2021.04.019

Boros, B. D., Greathouse, K. M., Gentry, E. G., Curtis, K. A., Birchall, E. L., Gearing, M., et al. (2017). Dendritic spines provide cognitive resilience against Alzheimer's disease. *Ann. Neurol.* 82, 602–614. doi: 10.1002/ana.25049

Cardona, A., Saalfeld, S., Schindelin, J., Arganda-Carreras, I., Preibisch, S., Longair, M., et al. (2012). TrakEM2 software for neural circuit reconstruction. *PLoS One* 7:e38011. doi: 10.1371/journal.pone.0038011

Chandrasekaran, K., Stoll, J., Giordano, T., Atack, J. R., Matocha, M. F., Brady, D. R., et al. (1992). Differential expression of cytochrome oxidase (COX) genes in different regions of monkey brain. *J. Neurosci. Res.* 32, 415–423. doi: 10.1002/jnr.490320313

Constantinidis, C., Funahashi, S., Lee, D., Murray, J. D., Qi, X.-L., Wang, M., et al. (2018). Persistent spiking activity underlies working memory. *J. Neurosci.* 38, 7020–7028. doi: 10.1523/JNEUROSCI.2486-17.2018

Cork, L. C., Masters, C., Beyreuther, K., and Price, D. L. (1990). Development of senile plaques. Relationships of neuronal abnormalities and amyloid deposits. *Am. J. Pathol.* 137, 1383–1392.

Crimins, J. L., Wang, A. C. J., Yuk, F., Puri, R., Janssen, W. G. M., Hara, Y., et al. (2017). Diverse synaptic distributions of g protein-coupled estrogen receptor 1 in monkey prefrontal cortex with aging and menopause. *Cereb. Cortex* 27, 2022–2033. doi: 10.1093/cercor/bhw050

Cseré,p, C., Pósfai, B., Schwarcz, A. D., and Dénes, Á (2018). Mitochondrial ultrastructure is coupled to synaptic performance at axonal release sites. *eNeuro* 5: ENEURO.0390-17.2018. doi: 10.1523/ENEURO.0390-17.2018

Curtis, C. E., and D'Esposito, M. (2003). Persistent activity in the prefrontal cortex during working memory. *Trends Cogn. Sci.* 7, 415–423. doi: 10.1016/S1364-6613(03)00197-9

Dumitriu, D., Hao, J., Hara, Y., Kaufmann, J., Janssen, W. G. M., Lou, W., et al. (2010). Selective changes in thin spine density and morphology in monkey prefrontal cortex correlate with aging-related cognitive impairment. *J. Neurosci.* 30, 7507–7515. doi: 10.1523/JNEUROSCI.6410-09.2010

Eberle, A. L., Selchow, O., Thaler, M., Zeidler, D., and Kirmse, R. (2015). Mission (im)possible—mapping the brain becomes a reality. *Microscopy* 64, 45–55. doi: 10.1093/jmicro/dfu104

Fehr, T., Janssen, W. G. M., Park, J., and Baxter, M. G. (2022). Neonatal exposures to sevoflurane in rhesus monkeys alter synaptic ultrastructure in later life. *Neuroscience* 25:105685. doi: 10.1101/2022.03.08.483510

Funahashi, S., Bruce, C. J., and Goldman-Rakic, P. S. (1989). Mnemonic coding of visual space in the monkey's dorsolateral prefrontal cortex. *J. Neurophysiol.* 61, 331–349. doi: 10.1152/jn.1989.61.2.331

Galloway, C. A., and Yoon, Y. (2013). Mitochondrial morphology in metabolic diseases. *Antioxid. Redox Signal.* 19, 415–430. doi: 10.1089/ars.2012.4779

Glancy, B., Kim, Y., Katti, P., and Willingham, T. B. (2020). The functional impact of mitochondrial structure across subcellular scales. *Front. Physiol.* 11:541040. doi: 10.3389/fphys.2020.541040

Glavis-Bloom, C., Vanderlip, C. R., and Reynolds, J. H. (2022). Age-related learning and working memory impairment in the common marmoset. *J. Neurosci.* 42, 8870–8880. doi: 10.1523/JNEUROSCI.0985-22.2022

Goldman-Rakic, P. S. (1995). Cellular basis of working memory. *Neuron* 14, 477–485. doi: 10.1016/0896-6273(95)90304-6

Hao, J., Rapp, P. R., Janssen, W. G. M., Lou, W., Lasley, B. L., Hof, P. R., et al. (2007). Interactive effects of age and estrogen on cognition and pyramidal neurons in monkey prefrontal cortex. *Proc. Natl. Acad. Sci. U.S.A.* 104, 11465–11470. doi: 10.1073/pnas.0704757104

Hara, Y., Park, C. S., Janssen, W. G. M., Punsoni, M., Rapp, P. R., and Morrison, J. H. (2011). Synaptic characteristics of dentate gyrus axonal boutons and their relationships with aging, menopause, and memory in female rhesus monkeys. *J. Neurosci.* 31, 7737–7744. doi: 10.1523/JNEUROSCI.0822-11.2011

Hara, Y., Yuk, F., Puri, R., Janssen, W. G. M., Rapp, P. R., and Morrison, J. H. (2014). Presynaptic mitochondrial morphology in monkey prefrontal cortex correlates with working memory and is improved with estrogen treatment. *Proc. Natl. Acad. Sci. U.S.A.* 111, 486–491. doi: 10.1073/pnas.1311310110

Hara, Y., Yuk, F., Puri, R., Janssen, W. G. M., Rapp, P. R., and Morrison, J. H. (2016). Estrogen restores multisynaptic boutons in the dorsolateral prefrontal cortex while promoting working memory in aged rhesus monkeys. *J. Neurosci.* 36, 901–910. doi: 10.1523/JNEUROSCI.3480-13.2016

Harris, J. J., Jolivet, R., and Attwell, D. (2012). Synaptic energy use and supply. *Neuron* 75, 762–777. doi: 10.1016/j.neuron.2012.08.019

Ivannikov, M. V., Sugimori, M., and Llinás, R. R. (2013). Synaptic vesicle exocytosis in hippocampal synaptosomes correlates directly with total mitochondrial volume. *J. Mol. Neurosci.* 49, 223–230. doi: 10.1007/s12031-012-9848-8

Kasai, H., Matsuzaki, M., Noguchi, J., Yasumatsu, N., and Nakahara, H. (2003). Structure-stability-function relationships of dendritic spines. *Trends Neurosci.* 26, 360–368. doi: 10.1016/S0166-2236(03)00162-0

Kennedy, M. B. (2016). Synaptic signaling in learning and memory. *Cold Spring Harb. Perspect. Biol.* 8:a016824. doi: 10.1101/cshperspect.a016824

Kuwajima, M., Spacek, J., and Harris, K. M. (2013). Beyond counts and shapes: Studying pathology of dendritic spines in the context of the surrounding neuropil through serial section electron microscopy. *Neuroscience* 251, 75–89. doi: 10.1016/j.neuroscience.2012.04.061

Lee, C. T., Laughlin, J. G., Moody, J. B., Amaro, R. E., McCammon, J. A., Holst, M. J., et al. (2019). An open source mesh generation platform for biophysical modeling using realistic cellular geometries. *arXiv* [Preprint]. arXiv:1909.04781. doi: 10.1016/j.bpj.2019.11.3400

Lees, R. M., Johnson, J. D., and Ashby, M. C. (2020). Presynaptic boutons that contain mitochondria are more stable. *Front. Synaptic Neurosci.* 11:37. doi: 10.3389/fnsyn.2019.00037

Li, S., Xiong, G.-J., Huang, N., and Sheng, Z.-H. (2020). The cross-talk of energy sensing and mitochondrial anchoring sustains synaptic efficacy by maintaining presynaptic metabolism. *Nat. Metab.* 2, 1077–1095. doi: 10.1038/s42255-020-00289-0

Lisman, J. E., and Harris, K. M. (1993). Quantal analysis and synaptic anatomy—integrating two views of hippocampal plasticity. *Trends Neurosci.* 16, 141–147. doi: 10.1016/0166-2236(93)90122-3

Litvina, E., Adams, A., Barth, A., Bruchez, M., Carson, J., Chung, J. E., et al. (2019). BRAIN initiative: Cutting-edge tools and resources for the community. *J. Neurosci.* 39, 8275–8284. doi: 10.1523/JNEUROSCI.1169-19.2019

Liu, X., and Hajnóczky, G. (2011). Altered fusion dynamics underlie unique morphological changes in mitochondria during hypoxia–reoxygenation stress. *Cell Death Differ.* 18, 1561–1572. doi: 10.1038/cdd.2011.13

Meyer, D., Bonhoeffer, T., and Scheuss, V. (2014). Balance and stability of synaptic structures during synaptic plasticity. *Neuron* 82, 430–443. doi: 10.1016/j.neuron.2014.02.031

Miller, E. K., Lundqvist, M., and Bastos, A. M. (2018). Working memory 2.0. *Neuron* 100, 463–475. doi: 10.1016/j.neuron.2018.09.023

Morrison, J. H., and Baxter, M. G. (2012). The ageing cortical synapse: Hallmarks and implications for cognitive decline. *Nat. Rev. Neurosci.* 13, 240–250. doi: 10.1038/nrn3200

Morrison, J. H., and Baxter, M. G. (2014). Synaptic health. *JAMA Psychiatry* 71, 835–837. doi: 10.1001/jamapsychiatry.2014.380

Moss, M. B., Moore, T. L., Schettler, S. P., Killiany, R., and Rosene, D. (2007). "Successful vs. Unsuccessful aging in the rhesus monkey," in *Brain aging: Models, methods, and mechanisms frontiers in neuroscience*, ed. D. R. Riddle (Boca Raton, FL: CRC Press/Taylor & Francis).

Nyberg, L., Boraxbekk, C.-J., Sörman, D. E., Hansson, P., Herlitz, A., Kauppi, K., et al. (2020). Biological and environmental predictors of heterogeneity in neurocognitive ageing: Evidence from Betula and other longitudinal studies. *Ageing Res. Rev.* 64:101184. doi: 10.1016/j.arr.2020.101184

Olesen, M. A., Torres, A. K., Jara, C., Murphy, M. P., and Tapia-Rojas, C. (2020). Premature synaptic mitochondrial dysfunction in the hippocampus during aging contributes to memory loss. *Redox Biol.* 34:101558. doi: 10.1016/j.redox.2020.101558

Paxinos, G., Watson, C., Rosa, M., Petrides, M., and Tokuno, H. (2012). *The marmoset brain in stereotaxic coordinates.* London: Academic Press.

Pekkurnaz, G., and Wang, X. (2022). Mitochondrial heterogeneity and homeostasis through the lens of a neuron. *Nat. Metab.* 4, 802–812. doi: 10.1038/s42255-022-00594-w

Peters, A., Sethares, C., and Luebke, J. I. (2008). Synapses are lost during aging in the primate prefrontal cortex. *Neuroscience* 152, 970–981. doi: 10.1016/j.neuroscience.2007.07.014

Pierce, J. P., and Lewin, G. R. (1994). An ultrastructural size principle. *Neuroscience* 58, 441–446. doi: 10.1016/0306-4522(94)90071-x

Pierce, J. P., and Mendell, L. M. (1993). Quantitative ultrastructure of Ia boutons in the ventral horn: Scaling and positional relationships. *J. Neurosci.* 13, 4748–4763. doi: 10.1523/JNEUROSCI.13-11-04748.1993

Rossi, M. J., and Pekkurnaz, G. (2019). Powerhouse of the mind: Mitochondrial plasticity at the synapse. *Curr. Opin. Neurobiol.* 57, 149–155. doi: 10.1016/j.conb.2019.02.001

Smith, H. L., Bourne, J. N., Cao, G., Chirillo, M. A., Ostroff, L. E., Watson, D. J., et al. (2016). Mitochondrial support of persistent presynaptic vesicle mobilization with age-dependent synaptic growth after LTP. *Elife* 5:e15275. doi: 10.7554/eLife.15275

Świetlik, D., Białowąs, J., Moryś, J., and Kusiak, A. (2019). Computer Model of synapse loss during an Alzheimer's disease-like pathology in hippocampal subregions DG, CA3 and CA1—the way to chaos and information transfer. *Entropy* 21:408. doi: 10.3390/e21040408

Tao-Cheng, J.-H., Gallant, P. E., Brightman, M. W., Dosemeci, A., and Reese, T. S. (2007). Structural changes at synapses after delayed perfusion fixation in different regions of the mouse brain. *J. Comp. Neurol.* 501, 731–740. doi: 10.1002/cne.21276

Thomas, C. I., Keine, C., Okayama, S., Satterfield, R., Musgrove, M., Guerrero-Given, D., et al. (2019). Presynaptic mitochondria volume and abundance increase during development of a high-fidelity synapse. *J. Neurosci.* 39, 7994–8012. doi: 10.1523/JNEUROSCI.0363-19.2019

Todorova, V., and Blokland, A. (2017). Mitochondria and synaptic plasticity in the mature and aging nervous system. *Curr. Neuropharmacol.* 15, 166–173. doi: 10.2174/1570159X14666160414111821

Upright, N. A., and Baxter, M. G. (2021). Prefrontal cortex and cognitive aging in macaque monkeys. *Am. J. Primatol.* 83:e23250. doi: 10.1002/ajp.23250

van der Walt, S., Schönberger, J. L., Nunez-Iglesias, J., Boulogne, F., Warner, J. D., Yager, N., et al. (2014). scikit-image: Image processing in python. *PeerJ* 2:e453. doi: 10.7717/peerj.453

Wang, M., Gamo, N. J., Yang, Y., Jin, L. E., Wang, X.-J., Laubach, M., et al. (2011). Neuronal basis of age-related working memory decline. *Nature* 476, 210–213. doi: 10.1038/nature10243

Wang, X.-J. (2021). 50 years of mnemonic persistent activity: Quo vadis? *Trends Neurosci.* 44, 888–902. doi: 10.1016/j.tins.2021.09.001

Wimmer, K., Nykamp, D. Q., Constantinidis, C., and Compte, A. (2014). Bump attractor dynamics in prefrontal cortex explains behavioral precision in spatial working memory. *Nat. Neurosci.* 17, 431–439. doi: 10.1038/nn.3645

Yao, J., Hamilton, R. T., Cadenas, E., and Brinton, R. D. (2010). Decline in mitochondrial bioenergetics and shift to ketogenic profile in brain during reproductive senescence. *Biochim. Biophys. Acta* 1800, 1121–1126. doi: 10.1016/j.bbagen.2010.06.002

Yuasa, S., Nakamura, K., and Kohsaka, S. (2010). *Stereotaxic atlas of the marmoset brain.* Tokyo: National Institute of Neuroscience.